A Study on the Thermal Behaviour of Micron-Sized Aluminium Powder in Contact with Water

Xiaoliang Zhang * , Haidan Cao , Jiawei Fang , Jun Zhang , Lingyun Wang

Posted Date: 13 May 2026

doi: 10.20944/preprints202605.0911.v1

Keywords: micron aluminium particles; accumulated dust; heat source; aluminium-water reaction; thermal effect

 doi:10.20944/preprints202605.0911.v1

Article

A Study on the Thermal Behaviour of Micron-Sized Aluminium Powder in Contact with Water

Xiaoliang Zhang *, Haidan Cao, Jiawei Fang, Jun Zhang and Lingyun Wang

School of Urban Construction and Safety Engineering, Shanghai Institute of Technology, Shanghai 201418, China

* Correspondence: yyyzxl@126.com (X.Z.)

Abstract

Aluminium powder, an energetic material, is prone to thermal runaway upon water exposure under local heat sources, yet the nonadiabatic mechanisms of micron sized accumulated aluminium powder under localized heating remain unclear. This study employs a proprietary characterization platform to investigate the effects of particle size, water content, and local heat source power on heat transfer in the dry state and on parameters including induction time, onset temperature, peak heat release rate, and reaction heat during the induction and main reaction phases. In the dry state, decreasing particle size enhances effective thermal conductivity and accelerates temperature rise, whereas elevated local heat source power exacerbates thermal inertia. Under local heating upon water exposure, reduced particle size significantly enhances reactivity; the reaction heat of 2 μm powder reaches 983 J/g, approximately fourfold. As shown in Figure 9 that of 106 μm powder. Water content exhibits nonmonotonic regulation, with onset temperature minimizing at 25% water content and 66.4 °C and reaction heat peaking at 33%. Paradoxically, elevated local heat source power suppresses reaction intensity, and reaction heat at 10 W is one sixth of that at 2.5 W, attributed to rapid product layer densification and the steam film barrier effect shifting the controlling mechanism from chemical to diffusion control. A coupled multifactorial predictive model incorporating the three factors was established with R^2 of 0.92, providing data and guidance for aluminium powder storage hazard prevention.

Keywords: micron aluminium particles; accumulated dust; heat source; aluminium-water reaction; thermal effect

1. Introduction

As the non-ferrous metal with the highest global production and consumption, aluminium powder is widely used in fields such as propellants, metal fuels and catalytic systems due to its high energy density (approximately 29 $MJ \cdot kg^{-1}$), good storage stability and environmentally friendly combustion products [1]. However, during production, processing and storage, aluminium powder may become hydrated due to changes in ambient humidity or accidental water ingress. In the presence of localised heat sources, such as hot equipment surfaces or electrical sparks, this can easily trigger a runaway chain reaction involving the aluminium-water reaction, leading to fire or explosion incidents [2,3]. In particular, the wet aluminium powder explosion that occurred in Shanghai, China, in 2023 demonstrated that, once hydrated, aluminium powder remains in a state of heat accumulation under the influence of internal heat sources. Consequently, in-depth research into the mechanisms governing the thermal behaviour of aluminium powder under the combined influence of local heat sources and water holds significant theoretical and practical importance for the safe storage of aluminium powder and the prevention of accidents.

The heat transfer within the accumulated particles is significantly influenced by the particle size [4]. Studies have shown that particle size exerts a significant influence on the effective thermal conductivity: fine-grained aluminium powder, due to its dense packing and reduced inter-particle

 doi:10.20944/preprints202605.0911.v1

spacing, significantly increases the effective thermal conductivity (k_{eff}). Conversely, large-particle-size aluminium powder, due to its higher porosity, experiences enhanced natural convection of gas within the pores, leading to easier heat dissipation [5,6].

Regarding the aluminium powder–water reaction system, the reaction between aluminium and water is highly exothermic in thermodynamic terms, with a standard molar enthalpy change of approximately -837.3 kJ/mol. Theoretically, the complete reaction of one gram of aluminium can produce approximately 1.24 L of hydrogen gas [7]. The dense aluminium oxide passivation layer on the surface of aluminium particles prevents direct contact between water molecules and the active aluminium within, resulting in a relatively slow reaction at room temperature [8,9].Schoenitz et al. [10] and Nie et al. [11] systematically investigated the oxidation behaviour of aluminium particles and the interfacial mass transfer mechanisms in the presence of water. Saceleanu et al. [12] and Wang et al. [13] determined the kinetic characteristics of the aluminium-water reaction using calorimetry, dividing the reaction into three stages: hydrolysis of the aluminium oxide layer, chemically controlled reaction, and diffusion-controlled reaction.

Particle size, content of water, and heat source power are the three key factors affecting the thermal behavior of aluminum powder when exposed to water. With regard to the particle size effect, research by Dong et al. [14] indicates that the hydrogen production rate increases significantly as particle size decreases. Zhang et al. [15] revealed that smaller particles possess a larger specific surface area, providing more reaction sites for water molecules. However, the aforementioned studies have primarily focused on the reaction kinetics of dispersed aluminium powder. In the case of packed aluminium powder systems, a reduction in particle size not only increases the specific surface area but also significantly raises the packing density and reduces the porosity [5,6], thereby substantially enhancing the system's heat transfer efficiency and influencing the thermal behaviour of the aluminium powder's reaction with water. Regarding the influence of water content, the study by Pang et al. [2] revealed its sensitive effect on the reaction temperature and pressure of aluminium powder, finding that aluminium powder heats up most rapidly at 30% water content, whilst excess water above 50% inhibits violent reactions due to dilution effects and mass transfer hindrances. Regarding the mechanism of action of local heat sources, Arlington et al. [16] systematically reviewed the application characteristics of exothermic reaction formation as a local heat source in the fields of material joining and sealing, revealing the mechanism by which local heat sources achieve rapid local heating through self-propagating reactions. Knecht et al. [17], on the other hand, developed a heat transfer surrogate model to describe the quasi-steady-state thermal distribution characteristics of oscillating flow systems containing local heat sources. However, existing research has largely focused on the uniform reaction behaviour of nano-alumina or under high-temperature adiabatic conditions, whilst studies on the multi-factor synergistic mechanisms governing the hydrothermal behaviour of micron-sized aggregated alumina in the presence of water under the influence of local heat sources remain insufficient.

Based on this, this paper employs a proprietary platform for the quantitative characterisation of the thermal behaviour of aluminium powder upon contact with water to systematically investigate the heat absorption and release patterns of micron-sized aluminium powder in both dry and wet states under the influence of a local heat source. By quantitatively characterising the effects of particle size, water content, and heat source power on six key parameters—the time to onset of the reaction (t_{in}), onset temperature (T_{onset}), maximum heat release rate (q_{r_max}), time to reach maximum reaction rate (Time to $q_{r\text{-}max}$), heat of reaction ($Q_{reaction}$) and reaction duration (Duration time), this study has elucidated the microscopic mechanisms underlying the thermal behaviour of aluminium powder upon contact with water. It provides a theoretical basis and technical support for the safe storage, transport and accident prevention of aluminium powder.

 doi:10.20944/preprints202605.0911.v1

2. Experiment and Methods

2.1. Experimental Materials

For this experiment, high-purity aluminium powder produced by Sinopharm Group was selected, with a purity of 99%. Deionised water was used to ensure that the water was free from dissolved salts and metal ions. This prevented potential interference or errors in the reaction results, thereby improving the accuracy and reproducibility of the experimental data. To systematically investigate the influence of aluminium powder particle size on its thermal behaviour upon contact with water, this study selected five aluminium powder samples of different specifications. The median diameter (D_{50}) were 2 μm, 21 μm, 47 μm, 92 μm and 106 μm, respectively. These ranged from the sub-micron to the micron scale. A Bettersize 2600 laser particle size analyser was employed to quantitatively characterise the particle size distribution of each sample. The analyser used the dry measurement mode to avoid particle agglomeration caused by liquid-phase dispersion. As shown in Figure 1a-e, the samples predominantly exhibited a unimodal distribution. This indicated that the particle size range was relatively concentrated and that the particle size uniformity was good. In this study, the most frequently used sample was the 106 μm aluminium powder. Figure 1f shows the X-ray diffraction pattern of the 106 μm sample, indicating that it consists primarily of high-purity aluminium. All aluminium powder samples were treated in a vacuum oven at 50 °C for 2 hours prior to use. This minimised potential interference from ambient humidity on the reaction system. The morphological characteristics and elemental compositions of the samples were examined using a FEI Quanta 200 scanning electron microscope equipped with an EDAX TEAM energy dispersive X-ray spectrometer.

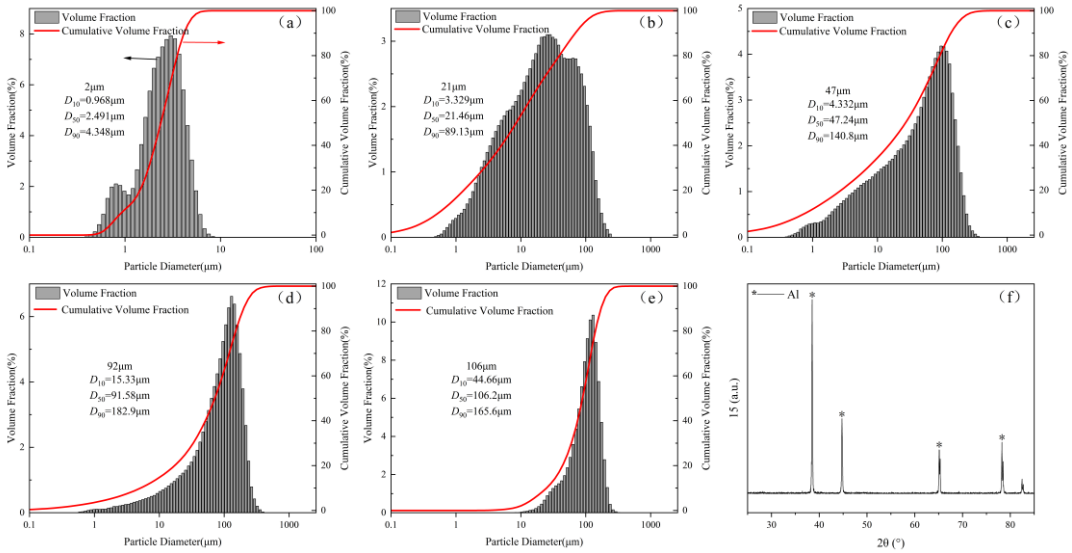

Figure 1. Characterization of experimental samples: (a)-(e) Particle size distribution of samples with sizes of 2μm, 21μm, 47μm, 92μm, and 106μm, (f) Composition analysis of the 106μm sample.

The rigorous screening and characterisation of the experimental materials laid a solid foundation for the subsequent precise investigation of the thermal behaviour of aluminium powders upon contact with water in the presence of a local heat source.

2.2. Experimental Setup

At an ambient temperature of 25 °C, the weighed aluminium powder sample is first placed in a glass reaction vessel. Deionised water is added in the specified proportion, and the mixture is stirred thoroughly to ensure uniform mixing of the solid and liquid phases. After sealing the reactor, it is purged with high-purity N_2. The bottom heating plate is then activated to heat the sample at a constant power, with continuous monitoring until the temperature and pressure stabilise. A

 doi:10.20944/preprints202605.0911.v1

proprietary platform designed for the quantitative characterisation of the thermal behaviour of aluminium powder upon contact with water was employed. A schematic diagram of the apparatus is shown in Figure 2. The platform primarily consists of a reaction vessel, a heating and temperature control system, a pressure sensor, a data acquisition and analysis platform, a safety interlock system and a control box. The reaction vessel is a borosilicate glass cylinder with an inner diameter of 13 mm and a height of 45 mm, with an aspect ratio of approximately 3.5. It is covered with a thermal insulation layer to minimise radial heat loss. A 0-10 W controllable heating element is positioned at the base to simulate a local heat source, with the power maintained at a constant level throughout the experiment. A K-type sheathed thermocouple is positioned at the centre of the aluminium-water mixture to monitor temperature changes in real time. A pressure sensor and a burst disc are installed at the top of the reactor to serve as overpressure protection devices. The system incorporates an atmosphere control module. Prior to the experiment, the system is purged with 99.9% high-purity N_2 for 10 minutes to eliminate oxygen interference.

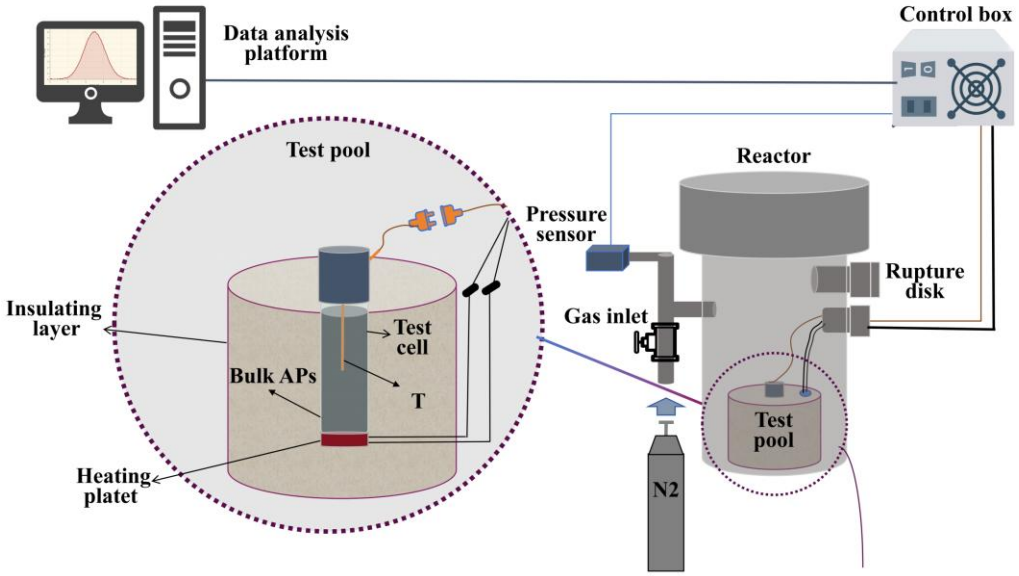

Figure 2. Platform for the quantitative characterisation of the thermal behaviour of aluminium powder upon contact with wate.

In the experiment, 3.00 g of aluminum powder was weighed and mixed according to a water-to-aluminum ratio ranging from 1:7.5 to 1:1, corresponding to moisture contents of 12%, 17%, 20%, 25%, 33%, and 50% [18]. Five aluminium powders with particle sizes of 2, 21, 47, 92 and 106 μm, as described in Section 2.1, were selected to investigate the effect of particle size on thermal behaviour under a fixed water content of 20% and a heat source power of 2.5 W. Three power settings (2.5, 5 and 10 W) were employed to examine the influence of heat source intensity. Blank control experiments were conducted simultaneously using dried aluminium powder and under low-power heat source conditions during the induction phase.

2.3. Analytical Methods

For both the dry aluminium powder system and the aluminium powder-water system (hereinafter collectively referred to as 'the system'), prior to the initiation of the reaction, the energy input from the heating element is equal to the sum of the heat stored within the system and the heat lost to the environment [19]. A non-adiabatic thermal model is established based on the law of conservation of energy, and the equilibrium relationship governing energy conservation in the system is shown in equation (1):

$$Q_{heat}=Q_{Al}+Q_{loss} \quad (1)$$

 doi:10.20944/preprints202605.0911.v1

where Q_{heat} is the energy input per unit time from the local heat source (J); Q_{Al} is the energy absorbed by the system for temperature rise (J), and Q_{loss} is the heat dissipated from the system (J).

The heat required to raise the system temperature can be expressed by equation (2) [20]:

$$Q_{Al}=cm\Delta T \tag{2}$$

The specific heat capacity of a mixture can be expressed using equation (3) [21]:

$$c=c_{Al}x_{Al}+c_{w}x_{w} \tag{3}$$

where, c_{Al} and c_w denote the specific heat capacities of aluminium powder and water, respectively, in kJ/(kg·K); c_{Al} = 0.88 kJ/(kg·K) and c_w = 4.18 kJ/(kg·K). x_{Al} and x_w denote the mass fractions of aluminium powder and water, respectively.

According to Newton's law of cooling [22], the rate of heat dissipation can be written as equation (4):

$$\frac{dQ_{loss}}{dt}=hA(T-T_0) \tag{4}$$

where h is the heat dissipation coefficient of the sample ($W\cdot m^{-2}\cdot °C^{-1}$), A is the heat dissipation surface area (m^2), T is the sample temperature (°C), and T_0 is the ambient temperature (°C).

Since the local heat source in this study employs a fixed heating power, differentiating equation (1) yields equation (5).

$$P=cm\frac{dT}{dt}+hA(T-T_0) \tag{5}$$

where P represents the heat source power (W). A relatively smooth curve from before the reaction is selected, and cm and hA are fitted using this equation.

Once the induction phase of aluminium powder i0n contact with water has concluded, the system enters a rapid reaction phase. The energy balance equation for this phase is given by equation (6).

$$P+mq_r=cm\frac{dT}{dt}+hA(T-T_0) \tag{6}$$

where q_r is the rate of exothermic reaction (W).

3. Results and Discussion

3.1. Effects of Heat Transfer in Powders

The heat transfer behaviour of piled aluminium powder under the influence of a local heat source forms the physical basis for understanding the mechanisms underlying the evolution of thermal runaway hazards. To eliminate the interference of chemical reactions and establish a baseline reference involving heat transfer processes alone, a systematic study was conducted on the temperature rise characteristics of dry aluminium powder under a constant bottom heat source power of 2.5 W. As shown in Figure 3a, under the influence of a constant local heat source, piled aluminium powder of different particle sizes exhibits distinct temperature rise characteristics. This difference primarily stems from the mechanism by which the particle size effect regulates the effective thermal conductivity of the powder bed. The spacing between particles decreases as particle size decreases. Consequently, the effective thermal conductivity increases as powder particle size decreases [23], thereby enhancing the efficiency of axial heat conduction and resulting in a faster rate of temperature rise and a higher steady-state temperature. Furthermore, the improved heat transfer efficiency in fine-particle powders promotes a more uniform temperature distribution within the bed, thereby exerting a critical influence on the induction time of the aluminium-water reaction system and its subsequent exothermic behaviour.

 doi:10.20944/preprints202605.0911.v1

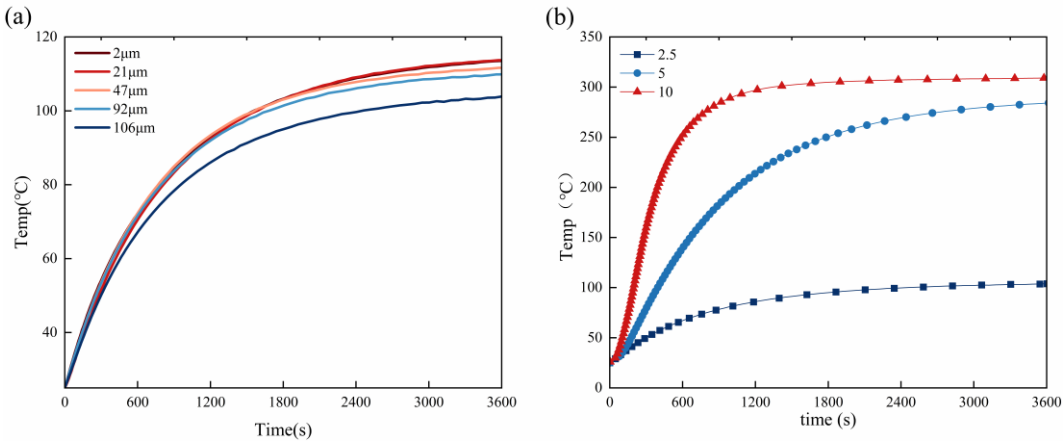

Figure 3. Temperature rise curve of aluminium powder as a function of particle size and heat source power.

Figure 3b illustrates the temperature rise characteristics of 106 μm aluminium powder under three different local heat source powers. Both the initial rate of temperature rise and the steady-state temperature show a significant positive correlation with the heat source power. When the power is increased from 2.5 W to 10 W, the steady-state temperature of the system rises sharply from 100 °C to 308 °C, whilst the time required to reach thermal equilibrium decreases correspondingly with increasing power. This thermal behaviour can be explained by the transient energy balance equation. As shown in equation (5), during the initial heating phase, the heat dissipation term is negligible and the heating rate is approximately proportional to the power. Consequently, as the heat source power increases, the initial heating rate of the aluminium powder increases significantly. Under high-power conditions, the bottom heat flux density increases significantly, leading to an intensified axial temperature gradient. Heat accumulates rapidly at the bottom of the powder bed, resulting in a pronounced thermal inertia effect [24,25]. As the temperature difference increases, the heat dissipation rate follows an exponential growth curve in accordance with Newton's law of cooling, until it reaches a steady state when it equals the heat source power. At this point, the steady-state temperature T_{ss} satisfies equation (7). These power-dependent heat transfer characteristics indicate that compacted aluminium powder exhibits a faster temperature rise response and a higher risk of thermal accumulation under the influence of localised high heat flux densities.

$$T_{ss}=T_0+\frac{P}{hA} \tag{7}$$

3.2. Effects of Water Content

Water content refers to the mass fraction of deionised water used in the reaction within the aluminium powder-water system. To investigate the effect of water content, experiments were conducted on aluminium powder-water systems with water contents of 12%, 17%, 20%, 25%, 33% and 50% under a 5 W local heat source. In this study, 12% and 17% were classified as low water content, 20% and 25% as medium water content, and 33% and 50% as high water content. As shown in Figure 4, the temperature curve of the reaction between aluminium powder and water exhibits phased characteristics. The induction phase involves a slow temperature rise, followed by a rapid reaction phase. After the reaction is complete, water evaporates under the influence of local heat sources, and the temperature rises again after the evaporation is complete. Water content influences the T_{onset} of the aluminium powder's reaction with water. When the water content varies within the range of 12% to 50%, T_{onset} exhibits a trend of first decreasing and then increasing. At a water content of 25%, T_{onset} is lowest, reaching 66.4 °C. At the same time, t_{in} shows a significant linear increase with increasing water content, and the fitting equation is given by equation (8).

$$y=6.55x+123.83 \tag{8}$$

 doi:10.20944/preprints202605.0911.v1

the correlation coefficient R^2 = 0.97, as shown in Figure 5a Based on the analysis in the preceding section, this linear relationship stems from the significant increase in the heat capacity of the mixed system. According to equation (3), when the water content increases from 12% to 50%, the specific heat capacity of the system rises from approximately 1.18 kJ/(kg·K) to 2.53 kJ/(kg·K), and the mass of the system increases accordingly. The high heat capacity significantly delays the time required for the system to reach the critical temperature for oxide layer rupture, thereby linearly extending the reaction induction period [26,27].

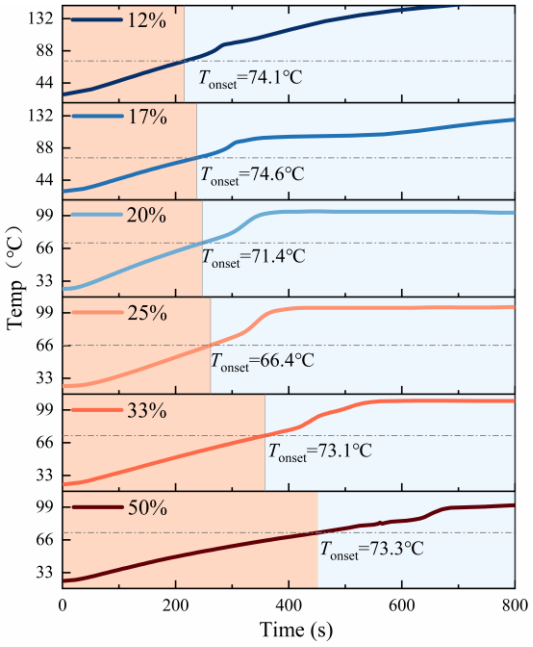

Figure 4. Changes in reaction temperature of aluminium powder at different water content.

The exothermic characteristics of the reaction exhibit a non-monotonic relationship with water content. As shown in Figure 5b, q_{r_max} peaks at 2.1 W/g at a water content of 17%, but drops to 1.3 W/g at a high water content of 50%. More crucially, $Q_{reaction}$ exhibits an inverted U-shaped distribution, rising initially and then decreasing. Specifically, as the water content increases from 12% to 33%, the heat release increases significantly from 42 J/g to 89 J/g, representing a 110% increase. However, upon further increase to 50%, the heat release actually decreases. This non-linear characteristic reflects the competing mechanisms of water playing dual roles as both a heat transfer medium and a reactant within the reaction system [28].

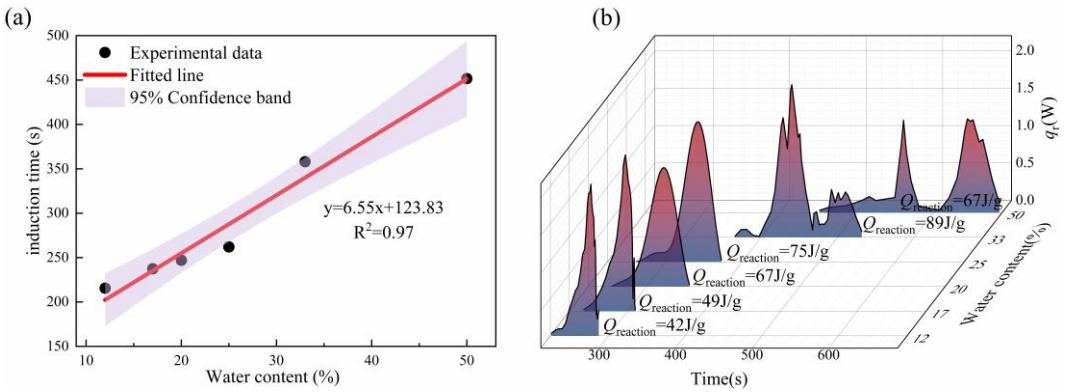

Figure 5. The induction time (a) and heat of reaction (b) of aluminium powder reaction under different water contents.

 doi:10.20944/preprints202605.0911.v1

In the low to medium water content range, an appropriate amount of water ensures that exposed aluminium nuclei come into sufficient contact with water molecules, thereby enhancing the reaction conversion rate. However, when the water content is too high, excess liquid water leads to an excessively large heat capacity of the system and the formation of a thick liquid film, increasing the diffusion resistance of water molecules towards the aluminium nucleus surface [29]. At the same time, the intense endothermic effect of evaporation enhances convective heat transfer losses, limiting the temperature rise of the system [30] More importantly, under high water content conditions, the layer of aluminium hydroxide produced by the reaction rapidly densifies, hindering the continued diffusion of water molecules towards unreacted aluminium nuclei and causing the reaction to terminate prematurely, as evidenced by a significant reduction in heat release [31,32].

3.3. Effects of Particle Size

To investigate the reaction characteristics of aluminium powder with different particle sizes, experiments were conducted using aluminium powders with particle sizes of 2 μm, 21 μm, 47 μm, 92 μm and 106 μm, under conditions of 20% water content and a local heat source power of 2.5 W. The reaction parameters and thermal effect parameters were analysed. Figure 6a shows the temperature rise of aluminium powders of different particle sizes upon contact with water, whilst Figure 6b reveals the variation in t_{in}, T_{onset}, Time to $q_{r\text{-}max}$, Duration time, $q_{r\text{-}max}$ and $Q_{reaction}$ with particle size. The experimental results indicate that tin increases significantly with increasing particle size. In this experiment, the induction time for 2 μm aluminium powder was 267 s, whereas that for 106 μm aluminium powder increased to 530 s. The induction stage primarily corresponds to the rupture of the oxide film and the formation of the reaction interface. On the one hand, fine aluminium powder particles have low thermal resistance and high heat transfer efficiency [33]. On the other hand, the smaller the aluminium particle size, the greater the surface area in contact with water during the reaction[34]. Consequently, the reaction rate during the induction phase is higher resulting in a significant reduction in t_{in}.

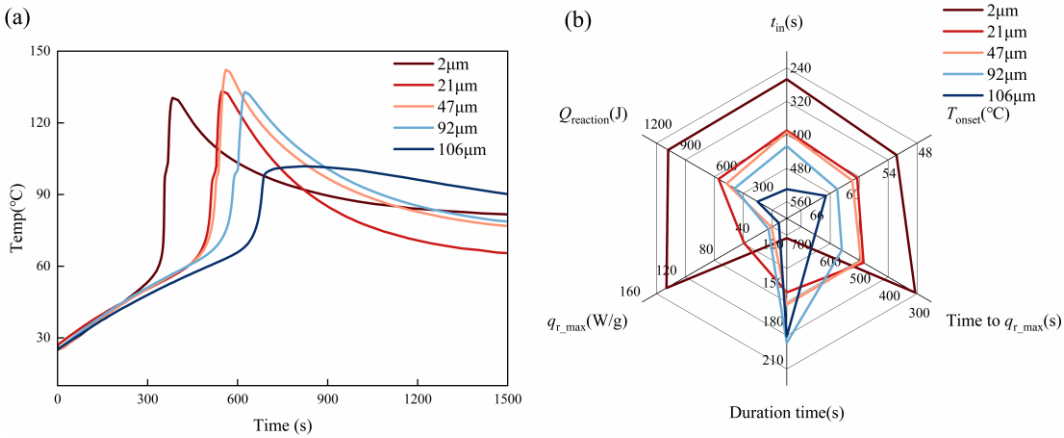

Figure 6. Temperature changes and thermal behaviour parameters during the reaction of aluminium powder of different particle sizes with water.

As the particle size of aluminium powder increases, the onset temperature of the reaction gradually rises. When the particle size is 2 μm, the T_{onset} is 49.8 °C, whereas it rises to 61.5 °C when the particle size is 106 μm. This trend indicates that aluminium powder with a smaller particle size is more readily capable of initiating a reaction with water at lower temperatures. This phenomenon is closely related to the stability of the oxide film on the surface of aluminium particles. A reduction in particle size significantly increases the specific surface area, providing more reaction sites and resulting in a significant energy difference between surface atoms and internal atoms, thereby enhancing reactivity [18,35]. At the same time, the reduction in particle size decreases the thermal

 doi:10.20944/preprints202605.0911.v1

inertia of the aluminium powder particles, accelerating the heating and destruction of the oxide film [36].

The effect of particle size on q_{r_max} is particularly pronounced. Figure 7 shows that the maximum heat release rate for aluminium powder with a particle size of 2 μm reaches 133.16 W·g^{-1}, whereas for a particle size of 106 μm, it is only 9.76 W·g^{-1}. As the particle size increases, the maximum heat release rate shows a significant downward trend. The reaction rate of metal particle hydrolysis is typically closely related to their specific surface area. Smaller aluminium powder particles provide a larger reaction interface, thereby significantly increasing the interfacial reaction rate. At the same time, small-particle sizes shorten the diffusion paths for heat and reaction products, facilitating the formation of a rapid autocatalytic process [37]. Furthermore, the time to q_{r_max} also increases significantly with increasing particle size, rising from 355 s for 2 μm particles to 694 s for 106 μm particles. This result indicates that larger aluminium powder particles not only exhibit a slower reaction initiation but also a slower reaction acceleration phase. This characteristic also explains the phenomenon whereby the duration time increases with increasing particle size.

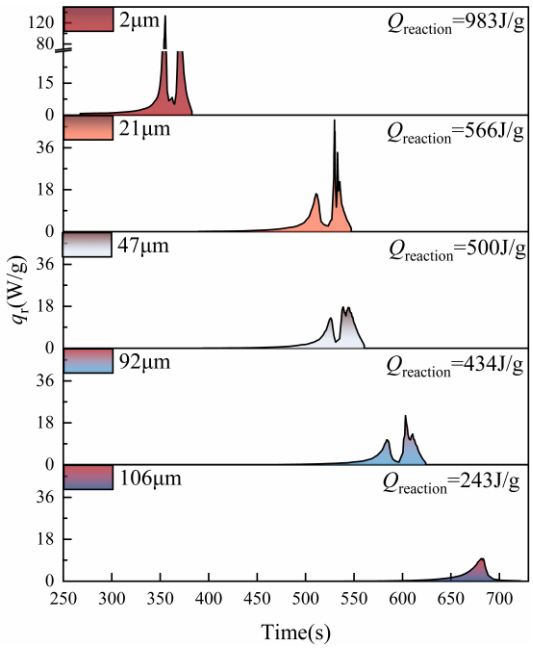

Figure 7. The heat of reaction during the reaction of aluminium powder of different particle sizes with water.

The $Q_{reaction}$ values for aluminium powders of different particle sizes also show marked differences. The reaction heat for 2 μm aluminium powder is 983 J·g^{-1}; when the particle size increases to 106 μm, the heat generated by the aluminium powder upon contact with water is 243 J·g^{-1}, which is only one-quarter of that for the smaller particles. This phenomenon is primarily due to the higher reaction conversion rate of the smaller particles. As the reaction proceeds, the generated layer of aluminium hydroxide gradually covers the surface of the aluminium particles and hinders further reaction [13]. When the particle size is larger, the dense product layer formed on its surface is more likely to completely encapsulate the aluminium core, effectively blocking the diffusion pathway for water molecules into the interior, causing the reaction to terminate prematurely and resulting in a significant reduction in the conversion rate [38,39].

The reaction of aluminium powder with water involves the rupture of the oxide film, interfacial heat transfer, and the generation and diffusion of hydrogen gas. In the early stages of the reaction, the oxide film on the surface of the aluminium particles ruptures under the influence of rising temperature or stress, thereby creating local reactive sites [40]. As the reaction between aluminium powder and water is exothermic, the heat generated further promotes the rupture of the oxide film and accelerates the reaction, resulting in a self-catalysing exothermic process. Furthermore, the hydrogen gas produced during the reaction forms bubbles on the particle surface. These bubbles alter

 doi:10.20944/preprints202605.0911.v1

the mass transfer conditions at the reaction interface, thereby further influencing the reaction rate. Due to their higher specific surface area and thinner oxide film [41], fine-particle-sized particles are more prone to forming the aforementioned autocatalytic reaction process, and consequently exhibit higher reaction activity and exothermic rates.

3.4. Impacts of Heat Sources

To systematically elucidate the regulatory mechanisms of heat source intensity on reaction kinetics, this study fixed the water content at 20% and the aluminium powder particle size at 106 μm, and conducted a comparative analysis of the initiation characteristics and exothermic behaviour of the aluminium powder's reaction with water under three heat source powers of 2.5, 5.0 and 10.0 W. The results are shown in Figure 8.

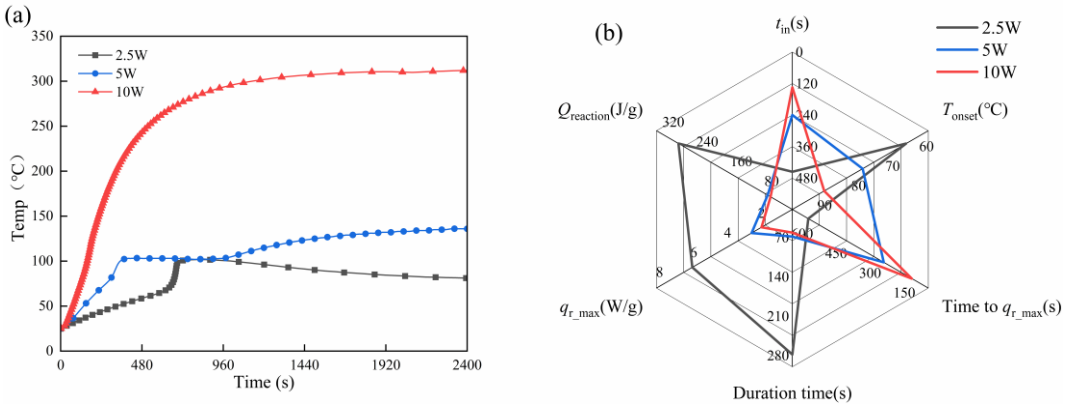

Figure 8. The temperature changes (a) and thermal behaviour parameters (b) during the reaction of aluminium powder with water under different heat source powers.

The temperature curve in Figure 8 reveals the significant influence of the heat source power on the system's temperature rise. When the heat source power was 2.5 W, the system exhibited a gradual temperature rise, with t_{in} lasting 530 s and T_{onset} at 61.5 °C. As the power was increased to 10.0 W, the initial rate of temperature rise increased significantly, and t_{in} was drastically reduced to 135 s. However, contrary to the trend of decreasing t_{in} content, T_{onset} rises monotonically with increasing power, reaching 84.6°C at 10.0 W—an increase of 23.1°C compared to the 2.5 W condition. The induction time of the aluminium powder-water reaction is influenced by ambient temperature, with the reaction rate exhibiting exponential growth with rising ambient temperature [28,34]. A high-power heat source causes a rapid rise in local temperature and, through heat transfer, leads to a rapid increase in ambient temperature. Compared to a low-power heat source, the reaction rate during the induction phase is accelerated, resulting in a significant reduction in t_{in}. At the same time, the increase in local heat source power increases the system's heating rate and enhances thermal inertia. The accumulation of heat requires a higher temperature to meet the reaction activation energy requirement, causing T_{onset} to shift towards higher temperatures [15].

The evolution of thermal behaviour parameters further corroborates the regulatory role of heat source power on the reaction process. In Figure 8b, the time to q_{r_max} decreases from 694 s at 2.5 W to 173 s at 10.0 W, whilst the duration time drops sharply from 192 s to 61 s, indicating that a high-power heat source not only accelerates the reaction but also concentrates the entire reaction process. Analysing the energy balance of a non-adiabatic reaction system, under the 2.5 W condition, the exothermic reaction and external heating form a positive feedback loop, allowing heat to accumulate effectively within the system and driving the reaction towards complete conversion. Under the 10.0 W condition, although the heat input is increased, the rapidly densifying product layer blocks the aluminium–water contact interface, causing the exothermic chemical process to be suppressed prematurely. Consequently, the system fails to fully utilise the chemical potential of the aluminium

 doi:10.20944/preprints202605.0911.v1

powder. This mechanism stands in stark contrast to the purely heat transfer-driven relationship observed in dry aluminium powder systems, where higher power leads to higher steady-state temperatures, highlighting the complex evolution of thermal behaviour once chemical reactions are introduced.

As shown in Figure 9, q_{r_max} decreases monotonically with increasing heat source power, falling from 9.76 W·g^{-1} at 2.5 W to 1.53 W·g^{-1} at 10.0 W. $Q_{reaction}$ also exhibits a significant downward trend, dropping sharply from 242.8 J·g^{-1} to 39.6 J·g^{-1}. For high-power heat sources, excessively high temperatures lead to an overly thick oxide layer, which hinders the interaction between water and aluminium. Consequently, both q_{r_max} and $Q_{reaction}$ for the aluminium-water reaction are reduced [42]. Concurrently, the vigorous evaporation of water vapour forms a vapour barrier on the particle surface, significantly increasing the mass transfer resistance of water molecules to the aluminium core. This shifts the reaction from being chemically controlled to diffusion-controlled, leading to premature termination of the reaction [43].

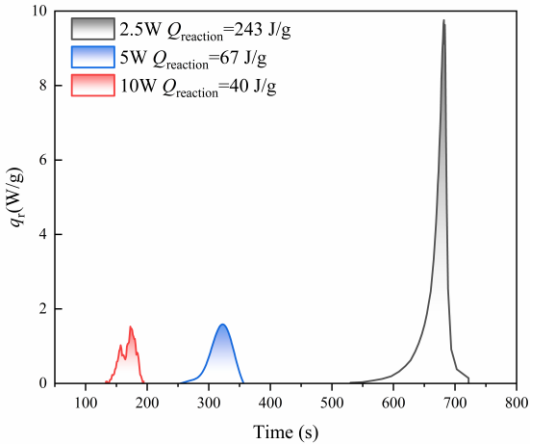

Figure 9. The heat of reaction during the reaction of aluminium powder with water under different heat source powers.

These findings have important implications for industrial safety and risk prevention. Low-power local heat sources in the 2.5 W range, such as the surfaces of equipment heating up slowly or poorly insulated pipes, although they delay the initiation of the reaction, are more conducive to the reaction proceeding to completion, which may lead to the accumulation of large amounts of hydrogen and the risk of delayed explosions. Conversely, high-power heat sources of the 10.0 W class, such as electrical sparks or mechanical friction hotspots, although reducing $Q_{reaction}$, trigger the reaction more rapidly, with t_{in} being approximately 135 s. Moreover, a high T_{onset} implies that the reaction is triggered whilst the system is in a higher energy state, potentially causing a violent pressure surge. Consequently, in aluminium powder storage environments, differentiated monitoring and control strategies must be established for local heat sources of varying power levels, with particular attention paid to the risk of hydrogen accumulation under conditions of low-power, prolonged exposure.

3.5. Modification of the Thermal Behaviour Model

The thermal behaviour of a bed of aluminium powder under the influence of a local heat source constitutes a system in which non-adiabatic heat transfer is coupled with a chemical reaction. Based on the principle of energy conservation, the temperature evolution of the system can be described by a lumped parameter model [44]. During the induction phase, the system satisfies equation (5), whilst during the reaction phase it satisfies equation (6). Integrating equation (6) yields:

$$\int P\mathrm{d}t + mQ_{reaction} = cm\Delta T + \int hA(T\text{-}T_0)\,\mathrm{d}t \tag{9}$$

 doi:10.20944/preprints202605.0911.v1

Non-linear regression calibration was performed based on the relative values of the total heat release per unit mass, $Q_{reaction}$, under various operating conditions, with aluminium powder particle size of 106 μm, water content of 20%, and power of 5 W taken as the reference conditions for normalisation. The experimental results presented earlier indicate that the mass fraction of water exerts a significant non-linear influence on the heat release from the reaction, exhibiting an inverted U-shaped profile. Based on the concept of multi-feature separation modelling[45], a quadratic polynomial regression was first used to fit the moisture correction factor $f(w)$ as shown in the following equation. The fitting results are illustrated in Figure 10a.

$$f(w)=-12.96w^2+9.21w-0.36 \quad (10)$$

in the equation, w represents the mass fraction of water. The fitted peak is at w = 0.35, with R^2 = 0.94. Taking w = 20% as the reference operating condition, the reaction heat is denoted as Q_0, and heat of reaction under the reference operating conditions described below is also denoted as Q_0.

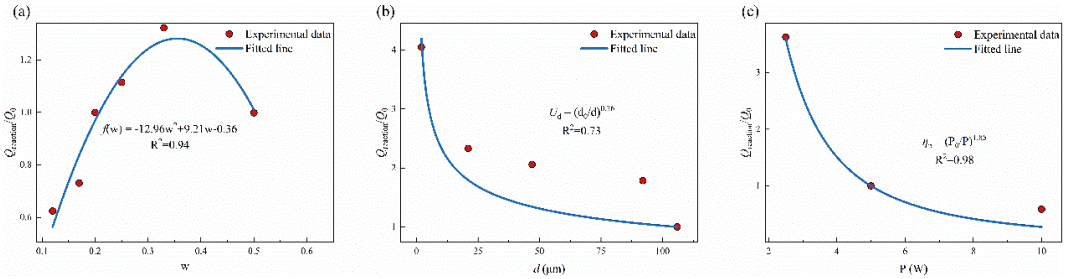

Figure 10. Comparison of experimental data with the fitted model.

In equation (3), the addition of water also affects the system's heat capacity:

$$cm=c_{Al}m_{Al}+c_w m_w \quad (11)$$

The dual mechanism of water's role in the thermal behaviour of the system. At low and moderate water contents, water acts as a reaction medium and enhances contact at the solid–liquid interface, thereby exerting a promoting effect. At high water contents, excess water increases the system's heat capacity, forms a liquid film that impedes mass transfer, and is accompanied by evaporative cooling, thereby exerting an inhibitory effect. These competing mechanisms collectively give rise to a non-monotonic water-control curve.

Particle size influences heat and mass transfer efficiency by modulating effective thermal conductivity and specific surface area. Based on the data in Figure 4, a power-law model [46] was used for fitting, as shown in Figure 10b. The particle size correction factor U_d obtained from the fitting is expressed as follows:

$$U_d=\left(\frac{d_0}{d}\right)^{0.36} \quad (12)$$

in the equation, d represents the median diameter, in μm. d_0 is the reference particle size, taken as 106 μm. R^2 = 0.73.

An increase in the heat source power P did not enhance the reaction rate. On the contrary, it reduced it. The suppression effect is described by introducing the power influence factor η_P, and a power law model is used for fitting, as shown in Figure 10c. The fitted η_P is expressed as follows:

$$\eta_P=\left(\frac{P_0}{P}\right)^{1.85} \quad (13)$$

in the equation, P_0 is the reference power, taken as 5 W. R^2 = 0.98, indicating a good fit. Under high-power conditions, the rate of temperature rise in the system is too fast, leading to rapid densification of the product layer. This transition from chemical control to diffusion control reduces the effective extent of the reaction.

Combining the above correction functions, the exothermic term of the reaction can be expressed as:

$$Q_{reaction}=Q_{r,0}\cdot f(w)\cdot U_d\cdot \eta_P \quad (14)$$

 doi:10.20944/preprints202605.0911.v1

in the equation, $Q_{r,0}$ represents the heat of reaction under reference conditions, which is 67 J/g. Substituting equation (10) to (14) into equation (9) yields the multi-factor coupled correction model:

$$\int P\mathrm{d}t + mQ_{r,0}(-12.96w^2+9.21w-0.36)\left(\frac{d_0}{d}\right)^{0.36}\left(\frac{P_0}{P}\right)^{1.85} = (c_{Al}m_{Al}+c_w m_w)\Delta T + \int hA(T-T_0)\,\mathrm{d}t \quad (15)$$

To verify the reliability of the established model, a comparative analysis was conducted between the total heat release predicted by the model and the experimentally measured values. The results indicate that the predicted values show good agreement with the experimental data, with an R^2 of 0.92 , demonstrating good overall predictive capability. The model can therefore be used for the quantitative prediction of heat release during aluminium powder–water reactions under various operating conditions.

Based on the coupled model of non-adiabatic heat transfer and aluminium-water reaction, this section introduces correction terms for water content and heat source power, constructing a coupled prediction model with clear physical significance. Through experimental data fitting, the nonlinear regulation effect of water, the power-law influence of particle size on the heat generation of aluminium powder upon water reaction, and the inhibitory mechanism of heat source power on reaction efficiency are quantified. This model not only enables quantitative prediction of the thermal behavior of aluminium powder upon water reaction but also provides a theoretical basis for thermal safety assessment during industrial storage and transportation.

4. Conclusions

Based on a proprietary platform for the quantitative characterisation of the thermal behaviour of aluminium powder upon contact with water, this study systematically reveals the thermal behaviour patterns and multi-factor synergistic regulation mechanisms of micron-sized accumulated aluminium powder reacting with water under the influence of a local heat source. Reducing particle size significantly shortened t_{in} and lowered T_{onset}, whilst markedly enhancing $Q_{reaction}$. the $Q_{reaction}$ of 2 μm powder reached 983 J/g, approximately threefold that of 106 μm powder, attributed to the larger specific surface area and higher effective thermal conductivity of fine particles promoting rapid oxide film rupture and subsequent autocatalytic exothermic processes. Water content exhibited nonmonotonic regulation of the reaction thermal behaviour, with T_{onset} minimising at 25% water content (66.4 °C) and $Q_{reaction}$ following an inverted U-shaped distribution peaking at approximately 33%. excess water reduced the conversion rate due to increased heat capacity and pronounced evaporative cooling effects that limited system temperature rise. Elevated heating power paradoxically suppressed reaction intensity, with $Q_{reaction}$ decreasing sharply from 242.8 J/g to 39.6 J/g as power increased from 2.5 W to 10.0 W, owing to rapid product layer densification forming a continuous passivation layer and the steam film barrier effect, which collectively shifted the rate-controlling mechanism from chemical control to diffusion control and caused premature reaction termination. A coupled multifactorial predictive model incorporating particle size, water content and heating power was established and rigorously validated against experimental data, achieving R^2 = 0.92 and demonstrating robust predictive capability for total reaction heat, thereby providing a theoretical basis for quantitative thermal safety risk assessment and hazard prevention during aluminium powder industrial storage and transport.

Author Contributions: Conceptualization, X.Z; methodology, H.C.; software, H.C.; validation, J.F.; data curation, L.W.; writing—original draft preparation, H.C.; writing—review and editing, H.C.; visualization, J.Z.; supervision, X.Z. All authors have read and agreed to the published version of the manuscript.

Funding: Please add: This research was funded by the National Natural Science Foundation of China (Grant No. 22308018).

Data Availability Statement: The original contributions presented in this study are included in the article. Further inquiries can be directed to the corresponding.

 doi:10.20944/preprints202605.0911.v1

Acknowledgments: In Thanks for the concerted efforts of the co-authors, the dedicated help of the instructors, and the financial support of the National Natural Science Foundation of China (Grant No. 22308018).

Conflicts of Interest: The authors declare no conflicts of interest.

References

1. Sopha, B.M.; Ma'mun, S. Economic Analysis and Environmental Assessment of Aluminum Debris Power Generator for Deployment to Communal-Scale Disaster Areas. *Heliyon* **2021**, *7*, e07264. https://doi.org/10.1016/j.heliyon.2021.e07264
2. Pang, L.; Li, C.; Liu, J.; Sun, S. Study on the Hydrogen Production Law and Reaction Kinetics Mechanism of Aluminum Powder Oxidation under Different Moisture Content Conditions. *Int. J. Hydrogen Energy* **2025**, *100*, 319-329. https://doi.org/10.1016/j.ijhydene.2024.12.303
3. Kirton, T.; Saceleanu, F.; Salehi Mobarakeh, M.; Kholghy, M.R. Cogeneration of Hydrogen, Alumina, and Heat from Aluminum-Water Reactions. *Int. J. Hydrogen Energy* **2024**, *68*, 115-127. https://doi.org/10.1016/j.ijhydene.2024.04.038
4. Luo, Y.; Gui, N.; Yang, X.; Jiang, S.; Liu, Z. Analytical Generalized Thermal Resistance Model for Conductive Heat Transfer in Pebble Beds Based on Heat Flux Weighted Temperature Difference. *Int. J. Heat Mass Transfer* **2025**, *236*, 126401. https://doi.org/10.1016/j.ijheatmasstransfer.2024.126401
5. Rodrigues, S.J.; Vorhauer-Huget, N.; Tsotsas, E. Effective Thermal Conductivity of Packed Beds Made of Cubical Particles. *Int. J. Heat Mass Transfer* **2022**, *194*, 122994. https://doi.org/10.1016/j.ijheatmasstransfer.2022.122994
6. Zhao, Y.; Zhang, H.; Cai, J.; Ji, S.; Li, D. A Prediction Model of Effective Thermal Conductivity for Metal Powder Bed in Additive Manufacturing. *Chin. J. Mech. Eng.* **2023**, *36*, 41-51. https://doi.org/10.1186/s10033-023-00840-6
7. Wang, L.; Wang, M.; Liu, P.; Liu, J. Combustion Behavior of Ethanol/Ether Molecules-Coated Al Nanoparticles with H2o Vapor by Non-Equilibrium Molecular Dynamics Simulations. *ACS Omega* **2023**, *8*, 35800-35808. https://doi.org/10.1021/acsomega.3c03315
8. Taraba, B.; Maršálek, R.; Podstawka, T. Two Aspects of Water in Self-Heating Risk of Aluminium Powders: Calorimetric Study. *J. Therm. Anal. Calorim.* **2022**, *147*, 11671-11677. https://doi.org/10.1007/s10973-022-11402-8
9. Li, Q.Z.; Zhang, G.Y.; Zheng, Y.N.; Liu, J.F.; Li, X.W. Investigation on the Correlations between Thermal Behaviors and Explosion Severity of Aluminum Dust/Air Mixtures. *Powder Technol.* **2019**, *355*, 582-592. https://doi.org/10.1016/j.powtec.2019.07.090
10. Schoenitz, M.; Chen, C.-M.; Dreizin, E.L. Oxidation of Aluminum Particles in the Presence of Water. *J. Phys. Chem. B* **2009**, *113*, 5136-5140. https://doi.org/10.1021/jp807801m
11. Nie, H.; Zhang, S.; Schoenitz, M.; Dreizin, E.L. Reaction Interface between Aluminum and Water. *Int. J. Hydrogen Energy* **2013**, *38*, 11222-11232. https://doi.org/10.1016/j.ijhydene.2013.06.097
12. Saceleanu, F.; Vuong, T.V.; Master, E.R.; Wen, J.Z. Tunable Kinetics of Nanoaluminum and Microaluminum Powders Reacting with Water to Produce Hydrogen. *Int. J. Energy Res.* **2019**. https://doi.org/10.1002/er.4769
13. Wang, X.; Li, G.; Eckhoff, R.K. Kinetics Study of Hydration Reaction between Aluminum Powder and Water Based on an Improved Multi-Stage Shrinking Core Model. *Int. J. Hydrogen Energy* **2021**, *46*, 33635-33655. https://doi.org/10.1016/j.ijhydene.2021.07.191
14. Dong, R.K.; Mei, Z.; Zhao, F.Q.; Xu, S.Y.; Ju, X.H. Molecular Dynamics Simulation on the Reaction of Nano-Aluminum with Water: Size and Passivation Effects. *RSC Adv.* **2019**, *9*, 41918-41926. https://doi.org/10.1039/c9ra08484c
15. Zhang, X.; Wang, L.; Tao, G.; Guo, R.; Fang, J.; Zhang, J.; Mao, H. Hydrogen Production from Aluminum-Water Reactions at Low Temperatures: Based on an in-Situ Two Powders of Different Particle Sizes. *Front. Energy Res.* **2024**, *12*, 1441155-1441170. https://doi.org/10.3389/fenrg.2024.1441155
16. Arlington, S.Q.; Fritz, G.M.; Weihs, T.P. Exothermic Formation Reactions as Local Heat Sources. *Annu. Rev. Mater. Res.* **2022**, *52*, 219-248. https://doi.org/10.1146/annurev-matsci-081720-124041

 doi:10.20944/preprints202605.0911.v1

17. Knecht, S.; Zdravkov, D.; Albers, A. Surrogate Models for Heat Transfer in Oscillating Flow with a Local Heat Source. *Fluids* **2023**, *8*. https://doi.org/10.3390/fluids8030080
18. Chen, H.; Yao, Q.; Liu, Q.; Liu, H.; Zhang, X. Effects of Moisture Content on the Minimum Explosible Concentration of Aluminum Powder and the Related Mechanism. *J. Energy* **2020**, *2020*, 1393891-1393900. https://doi.org/10.1155/2020/1393891
19. Richner, G.; Neuhold, Y.-M.; Papadokonstantakis, S.; Hungerbühler, K. Temperature Oscillation Calorimetry for the Determination of the Heat Capacity in a Small-Scale Reactor. *Chem. Eng. Sci.* **2008**, *63*, 3755-3765. https://doi.org/10.1016/j.ces.2008.04.048
20. Domen, S.D. Heat Loss Compensated Calorimeter. *Nature* **1969**, *222*, 1061-1061. https://doi.org/10.1038/2221061a0
21. Grakov, T.; Mateev, V.; Marinova, I. Modeling the Energy and Heating Efficiency of 3d Printing for Composite Materials with Dispersed Volumetric Particles. *Electronics* **2025**, *14*, 688. https://doi.org/10.3390/electronics14040688
22. Zhao, B.; Liu, X. A Transient Formulation of Entropy and Heat Transfer Coefficients of Newton's Cooling Law with the Unifying Entropy Potential Difference in Compressible Flows. *Int. J. Therm. Sci.* **2024**, *205*, 109253. https://doi.org/10.1016/j.ijthermalsci.2024.109253
23. Persson, B.N.J.; Biele, J. Heat Transfer in Granular Media with Weakly Interacting Particles. *AIP Advances* **2022**, *12*. https://doi.org/10.1063/5.0108811
24. Joshi, K.A.; Raghavan, V.; Rangwala, A.S. An Experimental Study of Coal Dust Ignition in Wedge Shaped Hot Plate Configurations. *Combust. Flame* **2012**, *159*, 376-384. https://doi.org/10.1016/j.combustflame.2011.06.003
25. Zhang, J.; Wen, Y.; Wang, X.; Fang, J.; Zhang, X. Investigation of Temperature Gradient Effects and Effective Thermal Inertia During Adiabatic Decomposition of Substances with Varying Exothermic Characteristics. *Case Stud. Therm. Eng.* **2024**, *61*, 104896. https://doi.org/10.1016/j.csite.2024.104896
26. Yang, H.-L.; Li, Z.-S.; Ding, Y.-D.; Ge, Q.-Q.; Jiang, L. Hydrolysis Behavior and Kinetics of Aln in Aluminum Dross During the Hydrometallurgical Process. *Materials* **2022**, *15*. https://doi.org/10.3390/ma15165499
27. Khezri, A.; Raygan, S.; Amadeh, A.A. Investigating the Incubation Time of the Water Splitting Reaction between Aluminum Powder and Water. *Chem. Pap.* **2025**. https://doi.org/10.1007/s11696-025-04538-y
28. Trowell, K.; Goroshin, S.; Frost, D.; Bergthorson, J. Hydrogen Production Rates of Aluminum Reacting with Varying Densities of Supercritical Water. *RSC Adv* **2022**, *12*, 12335-12343. https://doi.org/10.1039/d2ra01231f
29. Fukui, T.; Yasuda, M.; Horie, T. Model Analysis of Mass Transfer in Liquid Films in a Taylor Flow Reactor for Gas-Liquid-Solid Three-Phase Reactions. *Chem. Eng. Process.: Process Intensif.* **2025**, *209*, 110151. https://doi.org/10.1016/j.cep.2025.110151
30. Bustos-Vanegas, J.D.; Martins, M.A.; Corrêa, P.C.; Baptestini, F.M.; de Oliveira, G.H.H. Modeling and Simulation of Coffee Bean Heating During Roasting: Effect of Heat Generation. *Front. Food Sci. Technol.* **2025**, *5*, 1603783. https://doi.org/10.3389/frfst.2025.1603783
31. Nie, H.; Schoenitz, M.; Dreizin, E.L. Calorimetric Investigation of the Aluminum–Water Reaction. *Int. J. Hydrogen Energy* **2012**, *37*, 11035-11045. https://doi.org/10.1016/j.ijhydene.2012.05.012
32. Razavi-Tousi, S.S.; Szpunar, J.A. Modification of the Shrinking Core Model for Hydrogen Generation by Reaction of Aluminum Particles with Water. *Int. J. Hydrogen Energy* **2016**, *41*, 87-93. https://doi.org/10.1016/j.ijhydene.2015.11.080
33. Mou, X.; Zhou, W.; Bao, Z.; Huang, W. Measurement and Theoretical Analysis of Effective Thermal Conductivity of Lanthanum Pentanickel Powder Beds for Hydrogen Storage in Different Particle Sizes and Bed Porosities. *J. Clean. Prod.* **2024**, *468*, 143098-143109. https://doi.org/10.1016/j.jclepro.2024.143098
34. Yavor, Y.; Goroshin, S.; Bergthorson, J.M.; Frost, D.L.; Stowe, R.; Ringuette, S. Enhanced Hydrogen Generation from Aluminum–Water Reactions. *Int. J. Hydrogen Energy* **2013**, *38*, 14992-15002. https://doi.org/10.1016/j.ijhydene.2013.09.070
35. Mao, H.-F.; Fang, J.-W.; Deng, Y.-K.; Zhang, J.; Zhao, Y.-L.; Feng, Y.; Xiong, M.; Gu, H.-T.; Feng, X.; Fang, J.-H.; Chen, J.-H.; Shu, C.-M.; Zhang, X.-L. Thermal Runaway Behaviour Induced by Localised Aluminium-Water Reaction at Low Temperature. *Chem. Eng. J.* **2026**, *533*, 174874-174886. https://doi.org/10.1016/j.cej.2026.174874

 doi:10.20944/preprints202605.0911.v1

36. Li, B.; Liu, H.; Gao, H.; Shu, C.-M.; Bi, M. Experimental Investigation of Moisture Content on Suppressing Ignition of Accumulated Dust. *Journal of Loss Prevention in the Process Industries* **2024**, *87*, 105209. https://doi.org/10.1016/j.jlp.2023.105209
37. Wang, Y.; Xu, K.; Li, L. Inhibition of the Reaction between Aluminium Dust and Water Based on the Him. *RSC Adv.* **2017**, *7*, 33327-33334. https://doi.org/10.1039/c7ra04787h
38. Gao, X.; Wang, C.a.; Bai, W.; Hou, Y.; Che, D. Aluminum-Based Fuels as Energy Carriers for Controllable Power and Hydrogen Generation—a Review. *Energies* **2022**, *16*. https://doi.org/10.3390/en16010436
39. Musicco, N.; Gelfi, M.; Iora, P.; Venturelli, M.; Artioli, N.; Montorsi, L.; Milani, M. A Review of Hydrogen Generation Methods Via Aluminum-Water Reactions. *Int. J. Thermofluids* **2025**, *27*, 101152-101173. https://doi.org/10.1016/j.ijft.2025.101152
40. Mezulis, A.; Richter, C.; Lesnicenoks, P.; Knoks, A.; Varnagiris, S.; Urbonavicius, M.; Milcius, D.; Kleperis, J. Studies on Water–Aluminum Scrap Reaction Kinetics in Two Steps and the Efficiency of Green Hydrogen Production. *Energies* **2023**, *16*, 5554. https://doi.org/10.3390/en16145554
41. Guo, H.; Zhang, W.; Pang, W. Preparation Technology, Reactivity and Applications of Nano-Aluminum in Explosives and Propellants: A Review. *Nanomaterials* **2025**, *15*, 1564. https://doi.org/10.3390/nano15201564
42. Buryakovskaya, O.A.; Vlaskin, M.S.; Grigorenko, A.V. Effect of Thermal Treatment of Aluminum Core-Shell Particles on Their Oxidation Kinetics in Water for Hydrogen Production. *Materials* **2021**, *14*, 6493. https://doi.org/10.3390/ma14216493
43. Soler, L.; Candela, A.M.; Macanás, J.; Muñoz, M.; Casado, J. Hydrogen Generation from Water and Aluminum Promoted by Sodium Stannate. *Int. J. Hydrogen Energy* **2010**, *35*, 1038-1048. https://doi.org/10.1016/j.ijhydene.2009.11.065
44. Csemány, D. Thermal Analysis of Suspended Single Droplet Evaporation Measurements with a Coupled Lumped Parameter Model. *Heat Mass Transfer.* **2023**, *59*, 2181-2195. https://doi.org/10.1007/s00231-023-03403-6
45. Shi, H.; Wang, S.; Fernandez, C.; Yu, C.; Xu, W.; Dablu, B.E.; Wang, L. Improved Multi-Time Scale Lumped Thermoelectric Coupling Modeling and Parameter Dispersion Evaluation of Lithium-Ion Batteries. *Appl. Energy* **2022**, *324*, 119789. https://doi.org/10.1016/j.apenergy.2022.119789
46. Martínez-Vargas, S.; Flores-Chan, J.-E.; Mandujano-Ramírez, H.-J.; Pérez-Montejo, S.; Calan-Canche, D.; Patino-Carachure, C. A Simple Study of Hydrogen Production from Recycled Aluminum Microparticles in Alkaline Media. *Hydrogen* **2026**, *7*, 55. https://doi.org/10.3390/hydrogen7020055